Integrated Modeling and Analysis of Physical Oceanographic and Acoustic Processes

Timothy F. Duda
Applied Ocean Physics and Engineering Department, MS 11
Woods Hole Oceanographic Institution, Woods Hole, MA 02543
phone: (508) 289-2495 fax: (508) 457-2194 email: tduda@whoi.edu

James F. Lynch
Applied Ocean Physics and Engineering Department, MS 11
Woods Hole Oceanographic Institution, Woods Hole, MA 02543
phone: (508) 289-2230 fax: (508) 457-2194 email: jlynch@whoi.edu

Ying-Tsong Lin
Applied Ocean Physics and Engineering Department, MS 11
Woods Hole Oceanographic Institution, Woods Hole, MA 02543
phone: (508) 289-2329 fax: (508) 457-2194 email: ytlin@whoi.edu

Karl R. Helfrich
Physical Oceanography Department, MS 21
Woods Hole Oceanographic Institution, Woods Hole, MA 02543
phone: (508) 289-2870 fax: (508) 457-2181 email: khelfrich@whoi.edu

Weifeng Gordon Zhang
Applied Ocean Physics and Engineering Department, MS 11
Woods Hole Oceanographic Institution, Woods Hole, MA 02543
phone: (508) 289-2521 fax: (508) 457-2194 email: wzhang@whoi.edu

Harry L. Swinney
Department of Physics, C1610
University of Texas at Austin, Austin TX 78712
phone: (512) 471-4619 fax: (512) 471-1558 email: swinney@chaos.utexas.edu

John Wilkin
Department of Marine and Coastal Sciences,
Rutgers University, New Brunswick, NJ 08901-8521
phone: (848) 932-3366 fax: (732) 932-8578 email: jwilkin@rutgers.edu

Pierre F. J. Lermusiaux
Department of Mechanical Engineering
Massachusetts Institute of Technology, Cambridge, MA 02139
phone: (617) 324-5172 fax: (617) 324-3451 email: pierrel@mit.edu

Report Documentation Page

Form Approved
OMB No. 0704-0188

1. REPORT DATE	2. REPORT TYPE	3. DATES COVERED
30 SEP 2014		**00-00-2014 to 00-00-2014**

4. TITLE AND SUBTITLE	5a. CONTRACT NUMBER
Integrated Modeling and Analysis of Physical Oceanographic and Acoustic Processes	5b. GRANT NUMBER
	5c. PROGRAM ELEMENT NUMBER
6. AUTHOR(S)	5d. PROJECT NUMBER
	5e. TASK NUMBER
	5f. WORK UNIT NUMBER
7. PERFORMING ORGANIZATION NAME(S) AND ADDRESS(ES) **Woods Hole Oceanographic Institution,Applied Ocean Physics and Engineering,266 Woods Hole Road,Woods Hole,MA,02543**	8. PERFORMING ORGANIZATION REPORT NUMBER
9. SPONSORING/MONITORING AGENCY NAME(S) AND ADDRESS(ES)	10. SPONSOR/MONITOR'S ACRONYM(S)
	11. SPONSOR/MONITOR'S REPORT NUMBER(S)

12. DISTRIBUTION/AVAILABILITY STATEMENT
Approved for public release; distribution unlimited

13. SUPPLEMENTARY NOTES

14. ABSTRACT

15. SUBJECT TERMS

16. SECURITY CLASSIFICATION OF:			17. LIMITATION OF ABSTRACT	18. NUMBER OF PAGES	19a. NAME OF RESPONSIBLE PERSON
a. REPORT **unclassified**	b. ABSTRACT **unclassified**	c. THIS PAGE **unclassified**	**Same as Report (SAR)**	**25**	

Nicholas C. Makris
Massachusetts Institute of Technology
77 Massachusetts Avenue, Room 5-222
Cambridge, MA 02139
phone: (617) 258-6104 fax: (617) 253-2350 email: makris@mit.edu

Dick K. P. Yue
Department of Mechanical Engineering
Massachusetts Institute of Technology, Cambridge, MA 02139
phone: (617) 253- 6823 fax: (617) 258-9389 email: yue@mit.edu

Mohsen Badiey
College of Earth, Ocean, and Environment
University of Delaware, Newark, DE 19716
phone: (302) 831-3687 fax: (302) 831-3302 email: badiey@udel.edu

William L. Siegmann
Department of Mathematical Sciences
Rensselaer Polytechnic Institute, Troy, New York 12180-3590
phone: (518) 276-6905 fax: (518) 276-2825 email: siegmw@rpi.edu

Jon M. Collis
Applied Mathematics & Statistics
Colorado School of Mines, Golden, CO 80401
phone: (303) 384-2311 fax: (303) 273-3875 email: jcollis@mines.edu

John A. Colosi
Department of Oceanography,
Naval Postgraduate School, Monterey, CA 93943
phone: 831-656-3260, FAX: 831-656-2712,
phone: (512) 471-4619 fax: (512) 471-1558 email: jacolosi@nps.edu

Steven Jachec
Marine and Environmental Systems
Florida Institute of Technology, Melbourne, FL 32901
phone: (321) 674-7522 fax: (321 674-7212 email: sjachec@fit.edu

Award Number: N00014-11-1-0701
http://www.whoi.edu/sites/IODA

LONG-TERM GOALS

The long term goal is to improve ocean physical state and acoustic state predictive capabilities. The goal fitting the scope of this project is the creation of physics-based, broadly applicable and portable acoustic prediction capabilities that include the effects of internal waves, surface waves, and larger scale features, with an emphasis on continental shelf and slope regions.

OBJECTIVES

A fundamental objective is to improve knowledge of oceanographic processes that are known to be relevant to underwater acoustic conditions, yet are not completely understood, to shed light on predictability. Project-scale objectives are to complete targeted studies of oceanographic processes in a few regimes, accompanied by studies of acoustic propagation and scattering processes in those regimes. Internal gravity waves and other submesoscale features are of specific interest. There are many open questions regarding the processes of internal-wave formation and propagation in the presence of low-frequency and large-scale ocean features, to be pursued by the basic research efforts of this project.

An additional objective is to develop improved computational tools for acoustics and for the physical processes identified by the targeted studies to be important, including work on data-driven ocean flow models. Time-stepped three-dimensional (3.5D) and true four-dimensional (4D) computational acoustic models are to be improved, as well as the methods used to couple them with ocean flow models. Fully numerical ocean flow modeling will also be improved by coupling models having nonhydrostatic pressure (NHP) physics, data-driven regional models having hydrostatic pressure (HP) physics, and surface wave models. Stochastic acoustic prediction models will be developed. The entire suite of models is to be tested for acoustic prediction effectiveness using existing data sets.

APPROACH

The approach toward advancing the state of the art is to identify acoustically relevant ocean processes, to improve computational models that include these processes, and to eventually model the acoustic effects in detail, for comparison with existing data. The acoustical relevance of each aspect of the features generated by these processes is best obtained with state-of-the-art acoustics research using the latest tools, with some tools in need of refinement or development, which forms part of this project. The acoustical relevancy of the processes is intended to prioritize research into each process into a ranking that may differ from that obtained from ocean ecosystem, climate, or ocean biogeochemical cycle research. The research plan anticipates feedback: as the acoustics research evolves, the goals and priorities in the process research plan may change.

This approach has been broken into seven tasks directed toward two goals, equivalent to the objectives listed above: (Goal #1) Development of integrated tools for joint oceanography/acoustic study and prediction, i.e. a modeling system; and (Goal #2) Develop an understanding of the physics of coastal linear and nonlinear internal wave generation and transformation, as observed in the model, lab and field-measured features, coupled with study of acoustical propagation in these features.

Achieving Goal #2 is intimately linked with the creation of modeling tools (satisfying Goal #1) because of the need to address the open questions on coastal internal wave physics, on coastal flow features, on details of NHP fluid computational modeling, and on coastal acoustic propagation effects. Each of the seven tasks is handled by a subset of the 15 total PI's. (The subsets intersect.) The name "Integrated Ocean Dynamics and Acoustics" (IODA) was given to the project at the initial PI meeting.

IODA project goal 1 tasks: Modeling tools

1. *NHP ocean model nested within data-driven HP model, tied to 4D acoustic models.* Under this task a nonhydrostatic physics computational flow model will be nested numerically within a spatial subdomain of data-assimilative hydrostatic physics regional flow model.
2. *Hybrid model: Hierarchical internal-wave models nested within HP model, tied to 3.5D acoustic models. (Also called composite physics model.)* Under this task, reduced-physics flow models capable of rapidly and efficiently modeling NHP nonlinear internal waves will be integrated with (nested within) regional flow models. These nested models can more rapidly compute internal wave positions and sizes than the full NHP model (Task 1), but may sacrifice detail and accuracy. Candidate models include those based on Korteweg-deVries type wave evolution equations and 2D NHP numerical models.
3. *Improved 4D deterministic and stochastic acoustic modeling.* Improvements to time-stepped 3D (3.5D) and 4D acoustic models will be made to increase speed and accuracy. A transport equation model for mean fields and higher order statistics will also be improved. The models will be coupled with the Task 1 and 2 models (i.e. will use output of those models as environmental condition input.)
4. *Unified waveguide model.* A prototype acoustic waveguide model solving for acoustic conditions in areas of rough seabed, internal fluid motions (including the nonlinear waves that form our main emphasis), and atmospherically forced rough surface waves will be developed. This coordinated effort is an attempt towards fully integrated physics, studying and solving for the dynamics of the ocean, surface and internal waves, and seabed and acoustics processes with atmospheric forcing, all in a fully synoptic and evolving fashion.
5. *Integration work necessary for the above.* Protocols for data output resolution, data format, metadata, and so on, will be developed. Protocols for physically correct nesting of the models with differing dynamics will be developed. Protocols for sufficient interpolation within the widely separated resolutions of the flow models and acoustic models will be established.

IODA project goal 2 tasks: Physics studies and model verification

6. *Spatially 3D internal-wave physics studies*. Basic research aimed at improving our knowledge of internal tide and nonlinear wave dynamics in 2D and 3D systems will be conducted using laboratory, theoretical and numerical models as appropriate, on a parallel track with the modeling tool development. These results will guide model development, testing, and use.
7. *Comparison of outputs and predictions with ground-truth field and lab data.* To gain understanding and confidence in the model fields, the generation, propagation, and dissipation of internal waves will be studied using laboratory experiments and direct numerical simulations of fluid flow (DNS). Additionally, for both the NHP and hybrid models, 3.5D acoustic effects will be modeled, analyzed and compared to experiment and field observations.

WORK COMPLETED

The end of FY 2014 corresponds to 3 years, 4 months completed in this project. Substantial progress has been made on many fronts The work completed thus far is reported here grouped according to the efforts of individual PIs or PI groups.

This year the fourth project IODA meeting was held at Woods Hole Oceanographic Institution (WHOI), 26-27 August, 2014. Eighteen project personnel attended, among them eleven PIs. Progress made to date and meaningful results were reported by many attendees. This information and other accomplishments are presented in the remainder of this report.

Acoustic model development (Tasks 3 and 5; Lin, Duda, Collis): Five new three-dimensional acoustic propagation codes in the MATLAB® programming environment have been completed thus far. Three of these are split-step Fourier (SSF) wide-angle parabolic equation (PE) codes at the typically used expansion order that is explained in papers by Thomson and Chapman [1] and Feit and Fleck [2]. The other codes are each unique, varying in expansion order and in method from the three standard-order SSF codes. These codes were completed in prior years and are described in the FY2013 report. The codes are not yet convenient to use nor are they easily interfaced to arbitrary ocean environment input fields. Making them easier to use would encourage their use and make their appropriate use (i.e. with proper setup to ensure correct output) more likely. Along these lines, trial protocols and codes have been written to interpolate ocean sound-speed fields onto the acoustic model grids. The system has been used for three different regional ocean model domains. The ocean sound-speed is not interpolated at the very fine acoustic model grid increment in the stepping direction (order one wavelength); instead, the resolution is three to six wavelengths. The required interpolation resolution, for a given accuracy, remains to be theoretically justified.

A new code for a marching PE algorithm that handles a non-flat water surface is being interfaced to the surface wave modeling activities of task 4. It was developed by Lin, and uses our new higher-order PE operator (Lin and Duda 2012), splitting of the differentiation operators, and an efficient "alternating direction implicit" calculation scheme. Figure 1 shows an example calculation. The code performance has been verified by comparison with benchmark solutions.

Ocean internal wave physics (Tasks 2 and 6; Helfrich): The work to date has investigated the joint effects of rotation and topography. Rotation causes the slow decay of an initial solitary wave due to inertia-gravity (IG) wave radiation. That radiated IG wave subsequently shoals behind the lead wave and forms a trailing packet of solitary-like waves. The initial wave also undergoes the usual fissioning process. A paper has been published, supported partially by this grant (Grimshaw et al., 2014). The paper includes weakly nonlinear theory based on the variable-coefficient Ostrovsky equation, numerical solutions of that equation, and MITgcm calculations. All the calculations are for a South China Sea setting. Future work is planned to compare South China Sea effects to New Jersey Shelf effects. ONR-sponsored studies have collected internal wave data at both the New Jersey Shelf and the South China Sea locations, allowing data/model comparison.

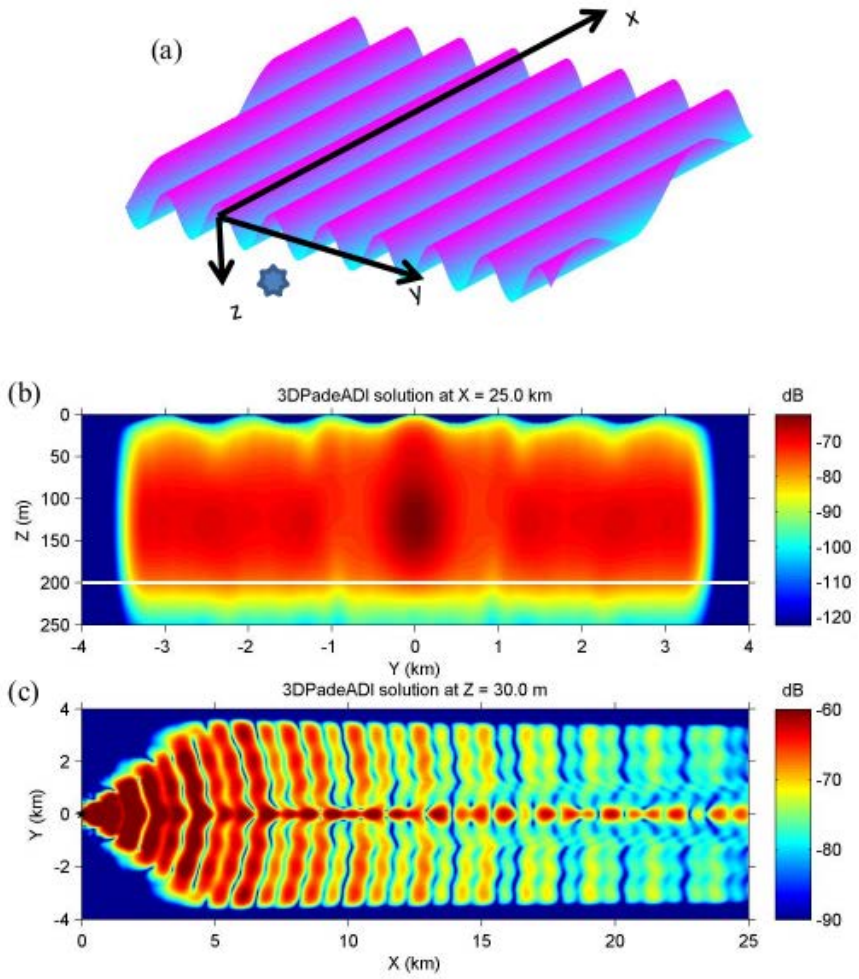

Figure 1. The ducting of sound by an idealized straight large ocean swell is shown, computed with the new 3D PE rough-surface code. (a) The geometry for the duct scenario is shown. The wave crests are aligned with the PE marching direction (x). (b) The transmission loss for 25 Hz at x= 25 km is shown. (c) The transmission loss at 30 m depth is shown. The ducting is evident in (b) and (c).

Unified ocean modeling (Tasks 2, 4 and 6; Yue, Liu, Lermusiaux): Drs. Dick Yue and Yuming Liu at MIT have worked to develop and validate a robust phase-resolved simulation capability for predicting the coupled dynamics of surface/internal waves with varying currents in littoral regions. An efficient algorithm enabling two-way coupling of nonlinear waves with varying currents was developed based on the use of Helmholtz decomposition. The coupled wave-current simulation capability was built up by integrating a nonlinear wave simulation tool (SNOW) with a current prediction tool (MSEAS primitive equation model). The verification of the capability was partially achieved. In particular, the effects of varying current on surface wave dynamics including focusing and defocusing of nonlinear waves were extensively investigated.

The MSEAS group of Dr. Lermusiaux has performed an analysis of salinity intrusions in the Middle Atlantic Bight shelfbreak region utilizing data and re-analyses for the SW06 experiment. The goal was to determine their types, properties, variability, generating mechanisms, and dynamics. Multiple salty

intrusions were identified, using the most recent multiscale reanalysis simulation described at (http://mseas.mit.edu/Research/SW06/MSEAS_reanalysis/2013_May07/). Intrusions were defined as mid-depth salinity maxima with salinities at or above 33.4 psu occurring over topography of 80 m or less depth. To test the impacts of tides, atmospheric forcing and data assimilation on the intrusions, several series of simulations were restarted from the above reanalysis at 10-day intervals. Each series consisted of four simulations: (i) without tides, (ii) without atmospheric forcing, (iii) without data assimilation and (iv), without tides, atmospheric forcing and data assimilation. Comparisons between each of these shorter simulations and the reanalysis were made, focusing on the intrusion events, identifying which process (tides, atmospheric forcing or data assimilation) had effects on the different intrusion events. The restart interval was chosen to prevent the time-space integrated ocean responses to the three forcings to excessively impact the dynamics and so alter the intrusions due to density (and not to one of the three forcings).

The MSEAS group evaluated the capability of their Navier-Stokes-Boussinesq non-hydrostatic finite volume (FV) code to capture the generation of internal waves (IW) from barotropic tidal flow over topography. This was done by comparing simulation results with published results of Khatiwala [3] and Legg and Huijts [4], which were obtained using the MITgcm. Some of the set-up differences between the FV simulations and those conducted with the MITgcm include: boundary conditions (BCs), forcing and parameterizations. Specifically, the MITgcm studies employed an upper free surface, radiative open BCs on the inlet and outlet, and a uniform sinusoidal body force to represent the barotropic tide. However, the FV code setup presently uses an upper rigid lid and time-dependent open BCs on the inlet and outlet to represent the forcing from the barotropic tide. Various simulations were compared to study how these set-up differences affect results.

The MSEAS group also utilized Dynamically Orthogonal (DO) equations to begin stochastic modeling of internal waves, specifically the influence of variability in the initial density profile on internal wave field generation and propagation.

The MSEAS high-order, non-hydrostatic, finite element and projection-based ocean code that utilizes the hybridizable discontinuous Galerkin (HDG) method was further designed, upgraded and verified (Mirabito, Haley and Lermusiaux, "Verification of high order hybridizable discontinuous Galerkin - projection schemes", manuscript in preparation; Ueckermann and Lermusiaux, "Hybridizable discontinuous Galerkin projection methods for Navier-Stokes equations", manuscript in preparation). This HDG code was used to analyze the dynamical response of phytoplankton and zooplankton to hydrostatic and non-hydrostatic Boussinesq physics (Ueckermann et al., "High order hybridizable discontinuous Galerkin projection schemes for 3D unsteady physical-biogeochemical ocean models", manuscript in preparation). Spatial discretization was done with horizontally unstructured, vertically structured (but time-dependent) grids using triangular and/or quadrilateral prismatic elements. Time integration employs modified implicit-explicit Runge-Kutta (IMEX-RK) schemes. A new selective nodal limiter, which is applied to stabilize the physics, was derived and implemented. To test this new HDG code, its output was compared to the hydrostatic MSEAS-PE and non-hydrostatic MITgcm, for the flow over an idealized Stellwagen Bank under varied Froude number (tidal amplitude) and Brunt-Väisälä frequency.

Ocean internal tide physics (Task 6; Swinney): In this effort, laboratory experiments and numerical simulations of internal wave generation and propagation are conducted for tidal flow over topography, as a function of tidal frequency ω and the vertical profiles of the buoyancy frequency, $N(z)$. Numerical simulations of the Navier-Stokes equations are conducted using a parallelized finite-volume based

solver and run on the University of Texas Stampede supercomputer, which makes it possible to achieve the large spatial dynamic range needed to span scales from short-wavelength nonlinear internal waves to the long wavelength internal tides. Laboratory experiments and simulations are being conducted for various topographic arrangements.

The group has developed a method to determine, *using only velocity field data*, the time-averaged energy flux and the total radiated power for 2-dimensional internal gravity waves. This was published in Lee et al. (2014). The power is computed using the stream function deduced from velocity field data. The method has been validated by comparing IW power determined by this method with IW power obtained from pressure field and velocity field data, and the results were found to agree within 1%. The stream function method for computing IW power has also been applied to laboratory data for the velocity field, and the results agreed well with numerical simulations that provided both the pressure and velocity fields. The method is now available to all in a Matlab code with a graphical user interface [Lee, Frank, "Internal Wave Stream Function Energy Flux and Power Calculator 5000", http://www.mathworks.com/matlabcentral/fileexchange/44833].

During the last two years the relationship between boundary currents generated by tidal flow over topography and the radiated internal wave power has been examined in experiments and in simulations of tidal flow of a uniformly stratified fluid over various topographies (knife-edge, tent, Gaussian, sinusoidal). Previous work used the hydrostatic approximation (where $N >> \omega$), while the present work examines situations where the hydrostatic approximation fails, as in the abyssal ocean, where N is small and comparable to, or even smaller than, ω (the M2 tidal frequency). Analysis of oceanic data has revealed that there are many ocean locations having $N < \omega$ (King et al., 2012). Recently, the group has examined conversion of tidal energy into radiating internal waves, particularly for cases with intense resonant boundary currents, which occur when a topographic slope matches the internal wave beam slope. It was found that this resonance phenomenon does not extend to the far field power radiated by internal waves. Kinetic energy density in boundary currents has often been used as a proxy to characterize the conversion of tidal energy to radiated internal wave power, but the present work shows that high boundary current energy density is a poor indicator of radiated power. A manuscript describing some of this work has been published (Dettner et al., 2013).

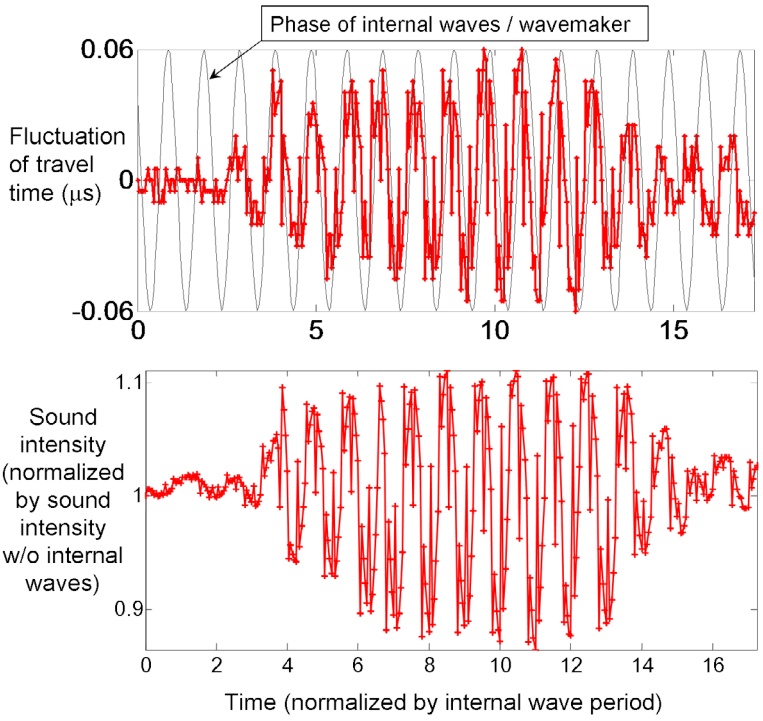

Figure 2. Fluctuations of sound travel time and intensity arising from the presence of internal waves in the acoustic path in the laboratory tank. With the arrival of an IW, the fluctuations grow for a few wave periods, and after the IW generator is switched off, the fluctuations decay for a few periods. The IW frequency is 0.14 Hz, the sound frequency is 1 MHz, and the buoyancy frequency of the stratified fluid is 0.25 Hz. The sound is generated and received by 12.5 mm diameter transducers separated by 0.16 m on a horizontal acoustic axis that is perpendicular to the IW beam.

Measuring and modeling sound fluctuations in internal waves (Tasks 3 and 7, Swinney and Lin): Laboratory experiments and modeling of sound propagation through an internal gravity wave field has been examined in a laboratory tank containing a density-stratified fluid. This work is ongoing. Dr. Likun Zhang, a postdoctoral researcher, plays a large role in this effort. Particle image velocimetry (PIV) using multiple cameras provides complete information on the internal wave field as input in sound propagation modeling and for interpreting the affect of IW on acoustic signals. Fluctuations of sound arrival time and intensity at the receiver have been measured for different conditions. Results from one experiment are shown in Figure 2.

The measured internal wave fields are compared with results from simulations of a 3-dimensional Navier-Stokes spectral code. The acoustic signals are analyzed in collaboration with Dr. Lin using a ray model and a 3D parabolic equation model. The goal is to understand sound propagating through and scattered by IW in an environment where all parameters can be controlled and varied. The results should guide computational model development for improved predictions of sound propagation in the oceans and should guide future field experiments as well.

Internal wave physics (Task 6, Swinney): Dr. Michael Allshouse, a postdoctoral researcher at U. of Texas at Austin, has completed an initial phase of studies of trapped cores within shoaling boluses. As

large-amplitude nonlinear internal waves approach the continental shelf, the waves form trapped cores of fluid (boluses) that move along the ocean bottom. Boluses have been observed along the Oregon shelf [5], where the leading bolus produced significant acoustic backscatter. Work continues, investigating the formation and evolution of boluses in laboratory experiments and simulations. In the experiments, internal waves are generated with a mode-one wave maker, and the development of these waves as they shoal is determined from velocity and density field measurements, using, respectively, particle imaging velocimetry and synthetic schlieren. The experiments are complemented by 2D and 3D direct numerical simulations. Results from the experiments and simulations will be analyzed using Lagrangian-based techniques to identify the boundaries of trapped cores. While previous analysis has used instantaneous snapshots of a flow, the Lagrangian approach used here will make possible a comprehensive exploration of bolus dynamics over time and will yield accurate identification of the bolus boundaries.

Ocean internal tide generation physics (Tasks 2 and 6; Zhang and Duda): The goal of effectively modeling internal waves must include reliable modeling of tidally-forced internal waves that appear at the tidal frequencies (internal tides). A study of internal tide generation made with ROMS [6] for supercritical continental slope geometry has been performed and was published this period (Zhang and Duda, 2013). Here, barotropic tidal flows force internal tides at the continental shelf edge, with the slope where the internal waves are generated being steep with respect to internal wave characteristics (i.e of supercritical slope) and the barotropic currents being slow with respect to internal wave speed (subcritical Froude number). The fields show signatures of significant nonlinear effects, some of which have undergone limited prior study, e.g. [7]. The effects are being studied by modifying nonlinear terms in the equation set (equation of state, momentum equation, turbulence closure). The internal tide energy is higher if nonlinear advection is included in the model, approximately double that seen with this nonlinear effect removed. The model treatment of subgrid-scale dissipation (nonlinear and irreversible) also has a large effect on the internal tide generation process. This work ties in well with the work of the U. Texas wave physics group [8], showing that incorrect handling of the nonlinearity is likely to compromise model comparisons with nature.

More recently, the ROMS study was expanded to study internal tides radiated from a canyon that is cut into the slope, a more fully 3D process. A full explanation of the processes responsible for the computed internal-tide beam pattern, which corresponds to observations in nature, has been published (Zhang et al., 2014). The explanation for variable generation efficiency in the canyon uses a model akin to the distorted-wave Born approximation. The explanation for the radiation pattern uses a phased-array internal tide extended-source argument that is common in acoustic engineering and signal processing, with the phase pattern governed by the bathymetry.

Improved analysis of field data (Task 7; Badiey): During SW06 [9], detailed measurements of the time-varying ocean environment were collected as acoustic signals were concurrently transmitted and received in the area. Using a mapping technique described in a journal paper from last year (Badiey et al., 2013), the three-dimensional (3D) temperature field for over one month of internal wave events was reconstructed. The results of this mapping are used for the statistical analysis of internal wave parameters, such as the wave propagation speed, direction, amplitude, and coherence length. The paper summarizes the results and also examines the implications for the acoustic field. The produced fields form a database useful for studying internal wave generation and propagation, and internal wave impact on 3D acoustic propagation.

Some internal wave statistical results were presented at the December 2013 Acoustical Society meeting. Some details are given here. A database of packet (event) properties was developed from thirty NLIW events recorded during the SW06 experiment. These data were obtained when each NLIW packet was located inside the thermistor farm (cluster of 18 central moorings) such that the initial front was close to the eastern edge of the farm. There are eight directly measured parameters and six derived parameters in this exercise. To the extent possible, John Apel's notation was followed in choosing these parameters. The mean value of each parameter, its standard deviation, and its estimated measurement error are listed in Table 1. The histograms of twelve parameters of the above set are shown in Figure 3.

H_1 is the depth of the warm surface layer, obtained by using the contour of the temperature at the middle of the thermocline as the reference. The value of H_2 (depth of the lower layer) follows immediately, with the total depth being 80 m. The soliton wavelength (λ_0) is the horizontal width between the troughs of the first two solitons. The histograms of the first two soliton amplitudes (η_1 and η_2) are shown in Figures 3f and 3g, respectively. For 61% of the events, the value of $\eta_1 > \eta_2$, and the amplitude decay constant is $\beta = \lambda_0^{-1} \ln(\eta_2/\eta_1) = 0.36$ km^{-1}. The half-amplitude width, *Ls*, is a characteristic scale of soliton that can be used to define the profile of these nonlinear waves. The number of solitons in a packet, *n*, is shown in Figure 3j. The NLIW propagation direction (α) is the direction measured within the thermistor farm with respect to true North. The average direction of the first group that contains 90% of the NLIW events is (309.5^o) nearly perpendicular to the shelf-bottom isobath contours. For the second group, containing only 10% of the event, this direction is 13.4^o, which is nearly parallel to the isobath contours. These waves are likely radiating from the Hudson Canyon area, rather than from the closest shelfbreak area. Assuming the NLIW speed within the thermistor farm is constant, we obtained that the propagation speed is 0.8 *m/s* falling into the range of its typical scale shown in Table 1.We next look at the slope of NLIW faces (designated as *K* here). Here we define $K = Ls/\eta_1$, with mean of 36.4 and histogram shown in Figure 3i. Using the measured NLIW propagation speed (v), the packet length (L) and spacing between packets (D) can be estimated by $L(i) = [T_n(i) - T_1(i)]v(i)$ and $D(i) = [T_1(i+1) - T_1(i)]v(i)$, where $T_1(i)$ and $T_n(i)$ are the times when the first and last soliton of the i^{th} NLIW packet arrive at the thermistor farm, respectively. The calculated results are shown in Figures 3k and 3l. The NLIW front curvature is another parameter of great importance when calculating 3D acoustic propagation. Here, we only recognized 4 NLIW events exhibiting obvious curved fronts within the thermistor farm area. Other events with the radius larger than 10 km exhibit almost straight NLIW fronts in this 4 km by 4 km area. The average value of R_c in the 4 events is 4.2 km.

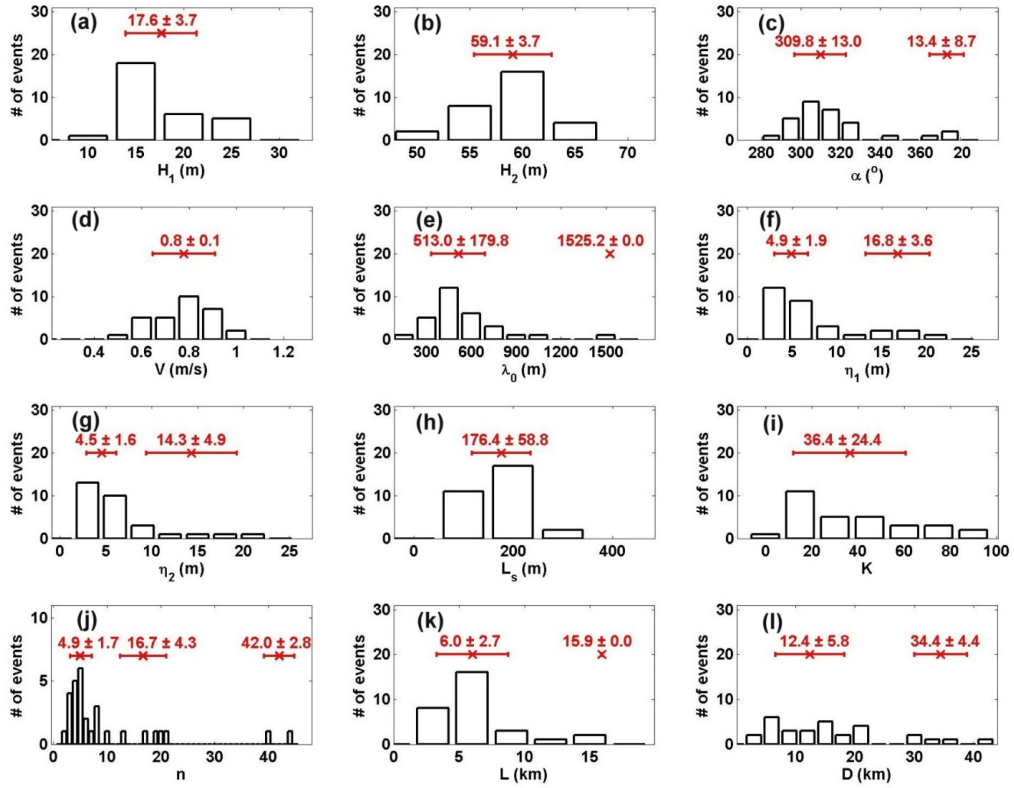

Figure 3. for the SW06 study, histograms of (a) Upper layer depth; (b) Lower layer depth; (c) Propagation direction with respect to true north; (d) Propagation speed; (e) Wavelength; (f) 1st soliton amplitude; (g) 2nd solition amplitude; (h) Soliton width; (i) Slope of NLIW faces; (j) Number of solitons in a packet; (k) Packet length; (l) Packet spacing.

Table 1. NLIW characteristic parameters

Characteristic(Symbol)	Unit	Typical Scale	SW06 Results	Uncertainty
Upper Layer Depth(H_1)	m	$5-25$	17.6 ± 3.7	2.4
Lower Layer Depth(H_2)	m	$30-200$	59.1 ± 3.7	2.4
Wavelength(λ_0)	m	$100-1000$	$513.0 \pm 179.8^{\square}$	5.0
1st Amplitude(η_1)	m	$0-30$	$4.9 \pm 1.9^{\square}$, $16.8 \pm 3.6^{\triangle}$	2.4
2nd Amplitude(η_2)	m	$0-30$	$4.5 \pm 1.6^{\square}$,$14.3 \pm 4.9^{\triangle}$	2.4
Solition Width(L_s)	m	100	176.4 ± 58.8	5.0
Number of Solitons(n)	$d.u.$	$1-20$	$4.9 \pm 1.7^{\square}$	2.2
			$16.7 \pm 4.3^{\triangle}$	4.1
			$42.0 \pm 2.8^{\Diamond}$	6.5
Direction(α)	$deg.(^o)$	a.s.	$309.5 \pm 13.0^{\square}$, $13.4 \pm 8.7^{\triangle}$	0.2
Speed(V)	m/s	$0.5-1.0$	0.8 ± 0.1	0.003
Slope of IW faces(K)	$d.u.$	$5-100$	36.4 ± 24.4	19.0
Packet Length(L)	km	$1-10$	$6.0 \pm 2.7^{\square}$, $15.9^{\triangle}$	0.02, 0.06
Packet Spacing(D)	km	$15-40$	$12.4 \pm 5.8^{\square}$, $34.4 \pm 4.4^{\triangle}$	0.04, 0.11
Decay constant(β)	km^{-1}	$0.1-1.0$	$0.36 \pm 0.33^{\star}$	$\star$
Radius of curvature(R_c)	km	$15-\infty$	$4.2^{\star}$	$\star$
Coherence length(L_{coh})	λ	$20-40$	$28.9 \pm 24.9^{\star}$	8.1

d.u. : dimensionless unit; a.s. : across shelf; λ : acoustic wavelength; $\star$: explaination in text;
$\square$: Group1; $\triangle$: Group2; $\Diamond$: Group3

In describing these statistics, we consider sources of error in the measurements and the parameter estimation, providing uncertainties. One likely source of measurement error is the discrete array element spatial and temporal spacing (resolution), and their element movement during the experiment (i.e. mooring motion). The accuracy of a particular parameter value would depend on the spatial position (in 3D) of the array farm in geotime. All the measurements during the passage of the NLIW are made using the same spatial and temporal variations. The uncertainties of the eleven parameters coming from the array elements vertical resolution (2.1 m), temporal resolution (15 sec) and their spatial movement (1.2 m in vertical and 5.0 m in horizontal plane) are obtained. The uncertainty of the number of solitons in a packet is comparable to the square root of the number according to Poison statistics. The calculated uncertainties are listed in the last column of Table 1.

Acoustic regimes and feature models (Tasks 2 and 3; Lynch and Colosi): Work has been done on developing simple analytical expressions for how various important acoustic quantities (horizontal array coherence length, transmission loss, scintillation index) depend on the parameters of the internal waves (and other coastal processes, such as fronts, eddies, spice.) With such "ocean feature model"-derived expressions, one can rapidly calculate acoustic parameter dependencies on ocean model parameters. Given "acceptability bounds" for error in the acoustic quantities, the models, in turn inform one as to how much error can be tolerated in the feature model parameters. This gives one some insight as to how much error in the output of a larger oceanographic model of ocean features is tolerable. The analytic model results also give easier insight into what the physics of the more complicated models is, and also a simple way to predict acoustically useful things like frequency dependence, and source to receiver geometry dependence. This approach is described in a general-audience paper published this year (Lynch et al., 2014).

Hierarchical hybrid model test bed (Task 2 and 5; Lynch, Helfrich, Lin, Duda): A part of the project that is organized by Arthur Newhall of WHOI is the interfacing of various ocean dynamics computational tools with acoustics computational tools, to form a test bed for acoustically relevant ocean dynamics research threads. A dimensionful version of the solver for the regularized version of the extended Korteweg-deVries equation with rotation (eKdVf, [10]) has been developed and is now embedded in our suite of codes. The eKdVf code is a wave evolution model for nonlinear and nonhydrostatic waves or other features, such as bores, that fit within an ocean waveguide normal-mode framework. The new version runs quickly and reliably. Precise behaviors of the quadratic-nonlinear version of this (KdVf) are the subject of a published paper (Grimshaw et al., 2014).

The background state governing the normal modes and the coefficients of the code, along with the initial waveform forcing at one end of the domain, are taken from data-driven ocean models such as MSEAS–Primitive Equation or ROMS, with a prototype interface in place for MSEAS. The design of the model is as follows: internal wave normal-mode speeds are taken from the data-driven model, after removing internal tides; internal wave mode rays are traced (with a few options for wave-mean flow interaction complexity and source location, wave source location being one of our research topics); coefficients for the eKdVf are evaluated along each ray; eKdVf is solved along each ray; the resulting high-frequency internal waves along each ray are mapped into a 3D space using interpolation schemes. 3D sound-speed fields are then ported to a 3D acoustic propagation models. Figure 4 shows an internal tide current field from the MSEAS data-driven model, some traced internal-tide rays (an unrealistic test arrangement intended for analysis of eKdVf behavior), and initial-condition internal-tide fields to be processed and then input to eKdVf as future work.

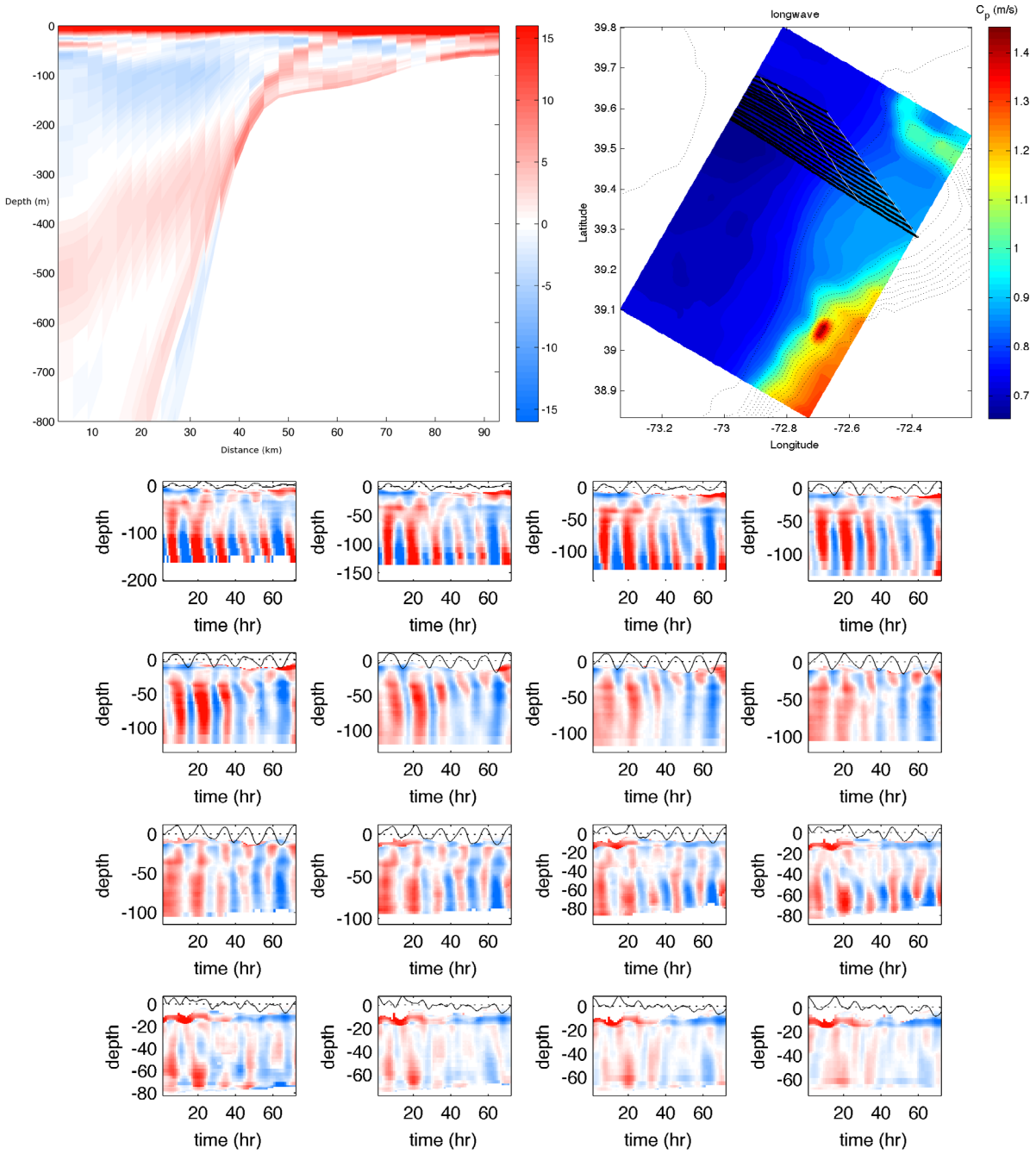

Figure 4. Plots are shown illustrating the interfacing the data-driven regional hydrostatic model, the internal tide raytrace model, and the KdV-type nonhydrostatic wave evolution model. (upper left) A time snapshot of upslope internal tide currents (cm/s) in a vertical slice spanning the supercritical continental slope zone from the MSEAS SW06 2012 reanalysis are shown. An internal tide beam is visible, lifting off the seabed over the shelf. (upper right). The long-wave internal tide mode=one speed is plotted in color. This is the simplest option for tracing internal tide rays neglecting current, current shear, and rotation, which may alter ray trajectories. The Hudson Canyon signature (deep water) is seen at the top right. Bathymetry is contoured (100-m step). Traced rays directed to the northwest are plotted. (bottom) A displacement time series (72 hours) at each ray starting point is shown. These must be converted to mode amplitude to serve as initial conditions to drive eKdVf along each ray. Red is westward current, blue eastward, with colors saturated at +/- 6 cm/s.

Nested ocean modeling (Task 2; Zhang, Wilken): Both the fully numerical (Task 1) and hybrid (Task 2) coastal internal wave modeling and analysis efforts require broad-scale ocean fields best obtained from data-driven modeling. The operational data-driven model for the northeastern US coast developed at Rutgers, the ESPreSSO model (http://www.myroms.org/espresso/), has been evaluated against independent CTD and glider data. The model has very good bias performance compared to other models for the region, showing that the anti-bias methods are effective. The model is also one of the best in terms of dynamical feature accuracy, showing low centered RMS difference values in various seasons and subsets of the domain. Work is underway toward two-way nested subdomains within the model that would have coverage and resolution required to effectively model internal tides and internal waves. The nested model would provide the regional fields needed for the hierarchical hybrid internal wave model and linked acoustic model. Figure 4 shows examples of simulated internal tides that would drive the hybrid model, although these are from the non-operational MSEAS model rather than the ESPreSSO model.

RESULTS

A few highlighted project results are presented here. Additional results such as internal tide breaking behavior and criterion (transition of internal tide to short internal waves), acoustic code tests, statistical acoustical modeling, and SW06 acoustic behavior in the field (ground truth study) will be presented in future grant reports or in reports for closely related grants.

Advanced ocean modeling (Lermusiaux): The first result of the MSEAS-based intrusion study mentioned earlier is that the salty intrusions considered (see Figs. 5 and 6) are mainly (sub)-mesoscale events, covering a significant portion of the Middle Atlantic Bight (MAB) shelf. (We are not studying intrusions controlled by double-diffusion effects, these processes are not modeled nor resolved in our 1km simulations.) The example of intrusions on Sep 24, 2006 (Figs. 5 and 6a) shows that intrusions are not occurring along a single potential density surface (confirmed by all events). A number of intrusion events were identified from specific cross sections. A few generating mechanisms were identified by the lack of intrusions (or changes in the intrusions) in the different restart runs. Some of these are shown in Table 2. One new specific process by which winds create some of these intrusions was identified. Briefly, winds blowing in a favorable direction can advect an upper layer mass of slope water onto the shelf. If subsequent (weaker) winds cause the subsequent offshore advection of a thinner surface layer, the bottom of the original onshore-advected water remains as an intrusion. Fig. 6 shows a pair of intrusion events in which the above wind mechanism is acting with modifications from other processes. In the Sep 24 event (Fig. 6a), when tidal forcing is present, more saline water is in position to be advected onshore; without tides, this added core was absent. In the Sep 13 event (Fig. 6b), there is an onshore finger that is absent without wind but there is also an offshore salty core that is present even when winds, tides and DA are all absent. This salty core is likely due to trapped slope-water meanders/eddies but may also be an effect of inertial oscillations.

For the evaluations of our 2D non-hydrostatic finite volume (FV) code, we compared the: (i) slope of the IW beams, (ii) velocity, and (iii) power spectra of the IW field. The stratification and slope of the IW beams (i), as well as power spectra conversion from the barotropic tide to the IW field (iii) agreed well. The magnitude of the velocity fields generally agreed very well, but differences were observed where the IW beams made contact with the upper and lower domain boundary. Internal waves reflected from the open boundaries were also noticeable. We implemented our modified sponge open boundaries which eliminated reflected waves.

Results from the DO simulations with varied number of modes and varied initial variance in density were evaluated for the linear background regime (weaker surface tides). Results were presented and found encouraging (not shown here).

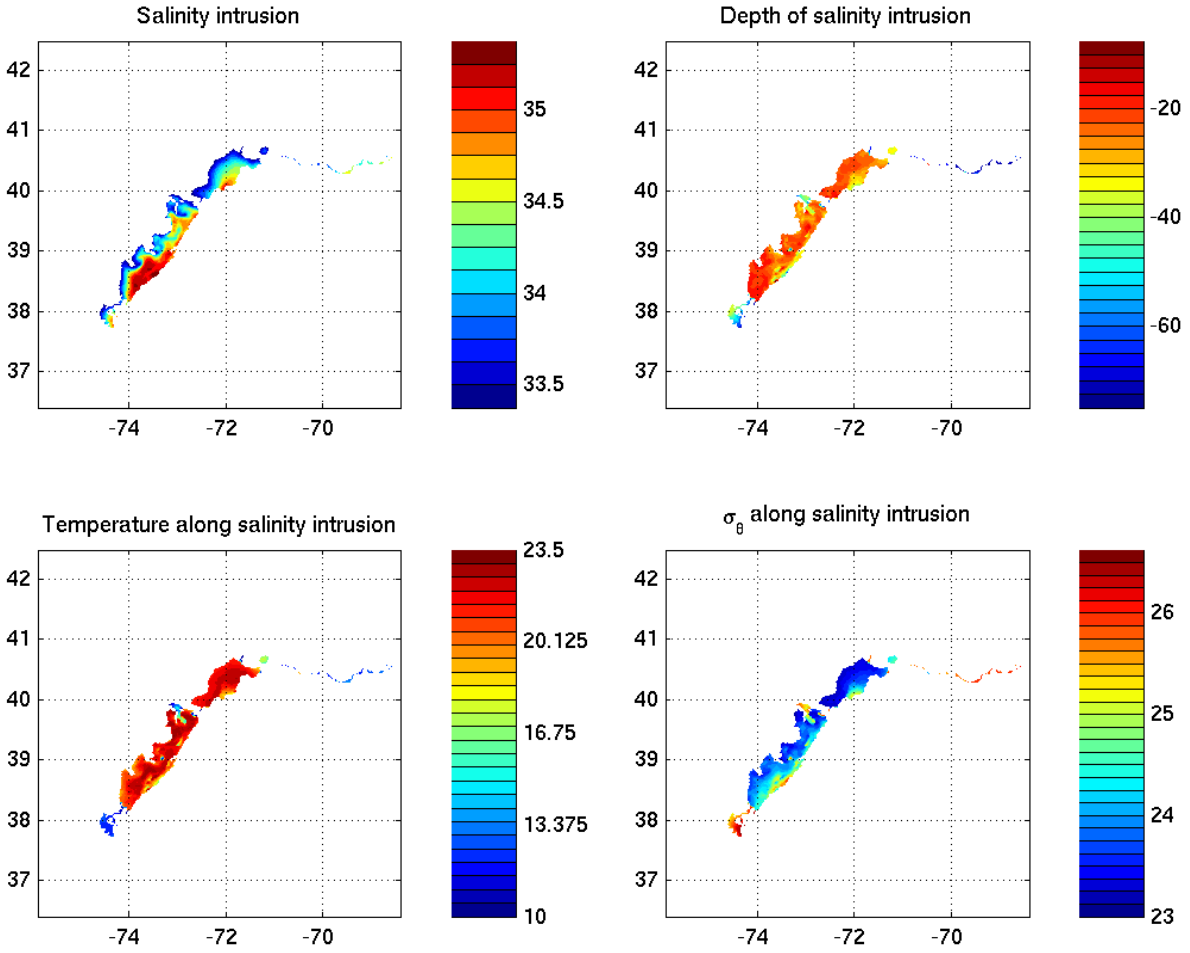

Figure 5. MAB shelf salinity intrusion on 24 Sept. 2006. Maps of salinity, temperature, depth and potential density anomaly along the mid-depth salinity maximum over the shelf. On this day, intrusions span most of the MAB and are not tied to a particular σ_θ (density) value.

Table 2. Some of the intrusion events detected in the high resolution domain	
Intrusions by the AWACS	**Intrusions by Hudson Canyon**
28 August (partly assimilation)	19 August (weak, wind)
4 September (partly assimilation)	24 August (weak, tides & wind)
17 September (partly assimilation)	13 September (wind & circulation)
20 September (wind)	24 September (wind)
24 September (wind & tides)	

For the HDG finite-element code, a key result was the rigorous derivation of consistent values for the dimensional and non-dimensional forms of the HDG stability parameter employed in the numerical fluxes (Ueckermann and Lermusiaux, "Hybridizable discontinuous Galerkin projection methods for Navier-Stokes Equations", manuscript in preparation) This consistent parameter is critical to ensure stability, accuracy, and numerical convergence. The results of the comparison of the 3DHDG code to the MSEAS-PE and MITgcm models in the Stellwagen Bank test are illustrated in Fig. 7. While the fields from all three codes are qualitatively similar, we note that that the two models with terrain-following coordinates limit the spurious noise in vertical velocity.

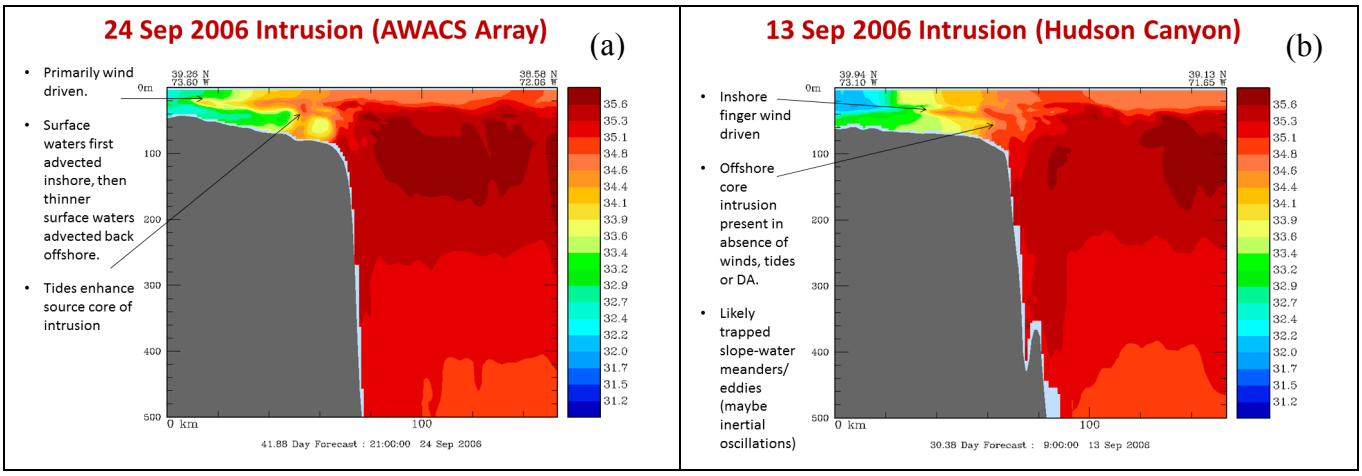

Figure 6. Salinity intrusion events. Vertical cross sections of salinity at two times/locations across the shelf/slope: (a) Mainly wind driven intrusion on 24 Sept. modified by tides. (b) A wind driven finger deeper on the shelf on 13 Sept., with an offshore core intrusion that arises from the density driven circulation. (The offshore intrusion is not due to winds, nor tides nor data assimilation.)

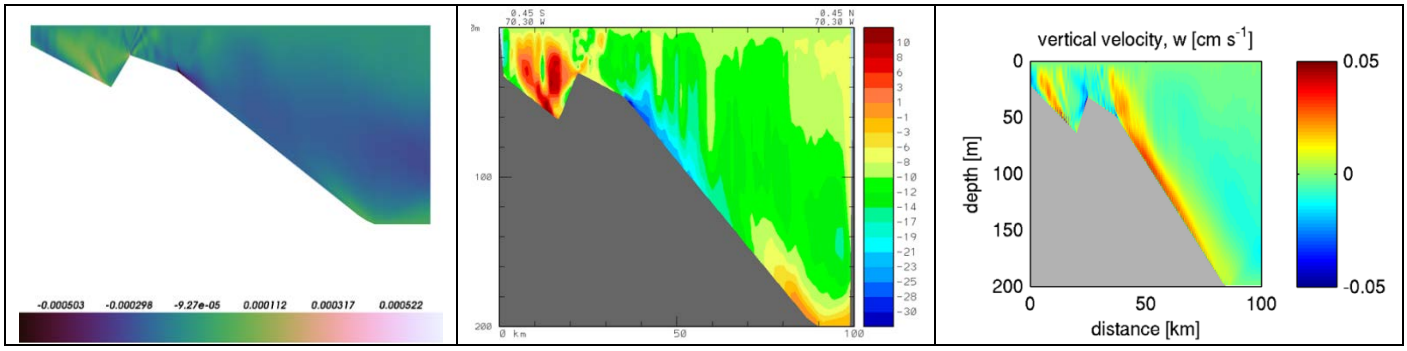

Figure 7. Vertical velocity slices over an idealized Stellwagen Bank, as computed by the (left) non-hydrostatic 3DHDG, (center) hydrostatic MSEAS-PE, and (right) non-hydrostatic MITgcm models.

Internal tide generation (Swinney): Research has found that a "virtual seafloor" in the real ocean suppresses internal wave generation below the level that one might naively predict. An understanding of internal waves (IW) in the oceans requires a determination of the conversion of tidal energy into internal wave energy. The University of Texas IODA group is investigating the dependence of the energy conversion on the ratio of the IW beam slope to the topographic slope, S_{IW}/S_{topo}. The top panel of Fig. 8 illustrates that in the abyssal oceans, where typically $S_{IW}/S_{topo} > 1$ for tall seamounts and ridges, the entire bottom topography contributes to the generation of internal waves. In contrast, for

moderate ocean depths (say less than 4 km), where typically $S_{IW}/S_{topo} < 1$ for seamounts and ridges, the radiated IW flux is generated only by the topography that rises above a local ***virtual seafloor***, as illustrated by the lower panel in Fig. 8, where wave interference reduces the conversion of tidal energy into IW energy. This work has recently been published (Zhang and Swinney, 2014). The research is being extended to 3D random topography. The goal is to use topographic data from the world's oceans to develop an accurate estimate of the global conversion of tidal energy into radiated IW power.

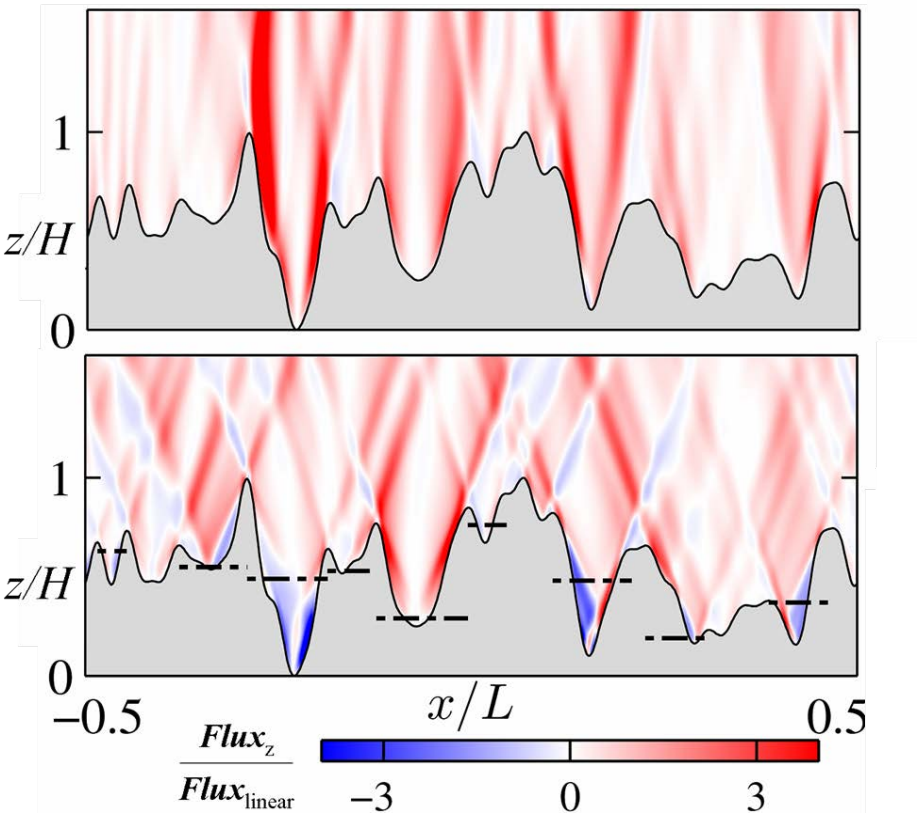

Figure 8. Time-averaged vertical energy flux of internal waves generated by tidal flow of stratified fluid over random topography, computed from a 2-dimensional numerical simulation of the Navier-Stokes equations for two different beam slopes S_{IW}, $S_{IW}/S_{topo} = 1.46$ (top) and 0.29 (bottom), where S_{topo} is the maximum topographic slope. In the upper panel internal waves are generated by the entire topography, while in the lower panel $S_{IW}/S_{topo} < 1$ and internal waves are generated only by topography above a local virtual seafloor, indicated by the dashed horizontal lines. The flux is normalized by that predicted from linear theory for weak topography. The random topography is generated from an ensemble of Gaussian random processes with a spectrum suggested by statistical modeling of the seafloor.

Internal tide generation (Zhang and Duda): The idea that nonlinear physics determines the energy ultimately found in internal tides at superctically steep slopes, and the internal tide phase, is supported by evidence in the Zhang and Duda 2013 paper. This means that linear models of internal tide generation, which are common, may be very good for some purposes, but may not be suited for detailed prediction of internal tides and the packets of nonlinear waves that they can spawn. That being, said, a linearized (but multiple-scatter) internal tide model has been successfully used to explain horizontal beam patterns of internal tides generated in canyons in fully nonlinear ROMS simulations (Zhang et al., 2014). Figure 9 shows in the center a toward-shore internal tide beam coming out of one

side of a canyon in a ROMS simulation, and shows at the right a similar result from an explanatory linearized model result. The model is a summation of mode-one Hankel-function waves from a line of sources along the so-called critical-slope locus, with the source amplitues and phases determind by a physical properties of the canyon bathymetry, the internal-wave phase speeds, and the internal-wave wavelengths. The waves coming out the side of the canyon are a feature that is consistent with some poorly-understood satellite images of internal waves at canyons, such as the one at the left in the figure. As a result of our work, we believe that linear models continue to have value to explain the physics of certain situations and to diagnose or differentiate internal-wave or internal-tide regimes, but may not be totally sufficient when wave phases (wave arrival times) are desired parameters in a prediction system (e.g. nonlinear wave packet positions, or arrival time at a specific locations, to be used for input to an acoustic model for for time-dependent acoustic system performance prediction).

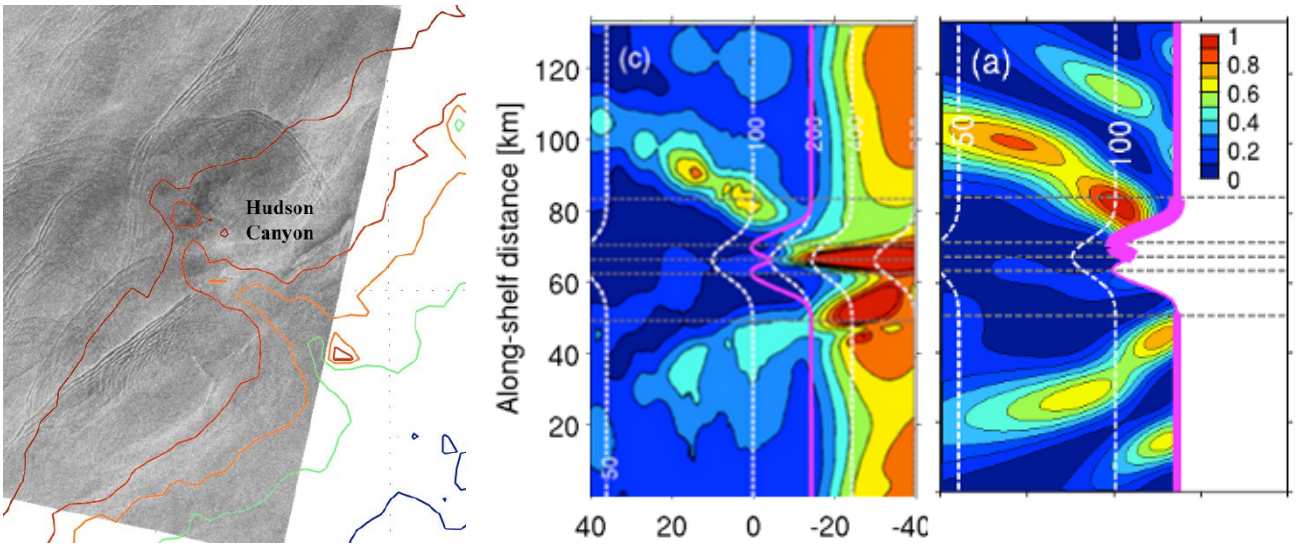

Figure 9. (left) An image extracted from Jackson [11] showing, in satellite synthetic aperture radar (SAR) data, internal waves traveling northward, which is to the right of Hudson Canyon when looking up the canyon. (center) A plot of normalized internal-wave (internal-tide) energy density in a numerical ROMS simulation of semidiurnal tidally forced flow at a canyon. Internal waves are seen to radiate from the canyon to the right as in the satellite image. Depth contours are in meters. (right) Internal-tide energy density from a semi-analytical mode-one internal-tide generation model. This model result matches the numerical result very well, considering the model simplicity.

Hierarchical hybrid model test bed (Task 2 and 5; Duda, Helfrich, Lynch, Lin): The first end-to-end calculation of acoustic conditions in small-scale internal-wave fields predicted using data-driven model conditions has been made, and was reported at the Spring Meeting of the Acoustical Society of America and the fall Oceans 2014 meeting. This prototype model used one shortcut, not taking initial conditions from internal tides in the data-driven model (plotted in Figure 4), but instead used sine-wave internal tides at the shelf break. Thus, best-possible predictions of internal-wave amplitudes and phases were not made, but "typical waves" were produced. These preliminary calculations were made to identify problems related to procedures such as tracking displacements of isotherms that disappear or appear over time, due to advection and/or surface fluxes, with poor tracking hobbling a de-tiding operation, to test run-time speeds, and to test interpolation methods. Figure 10 shows some images from the calculation.

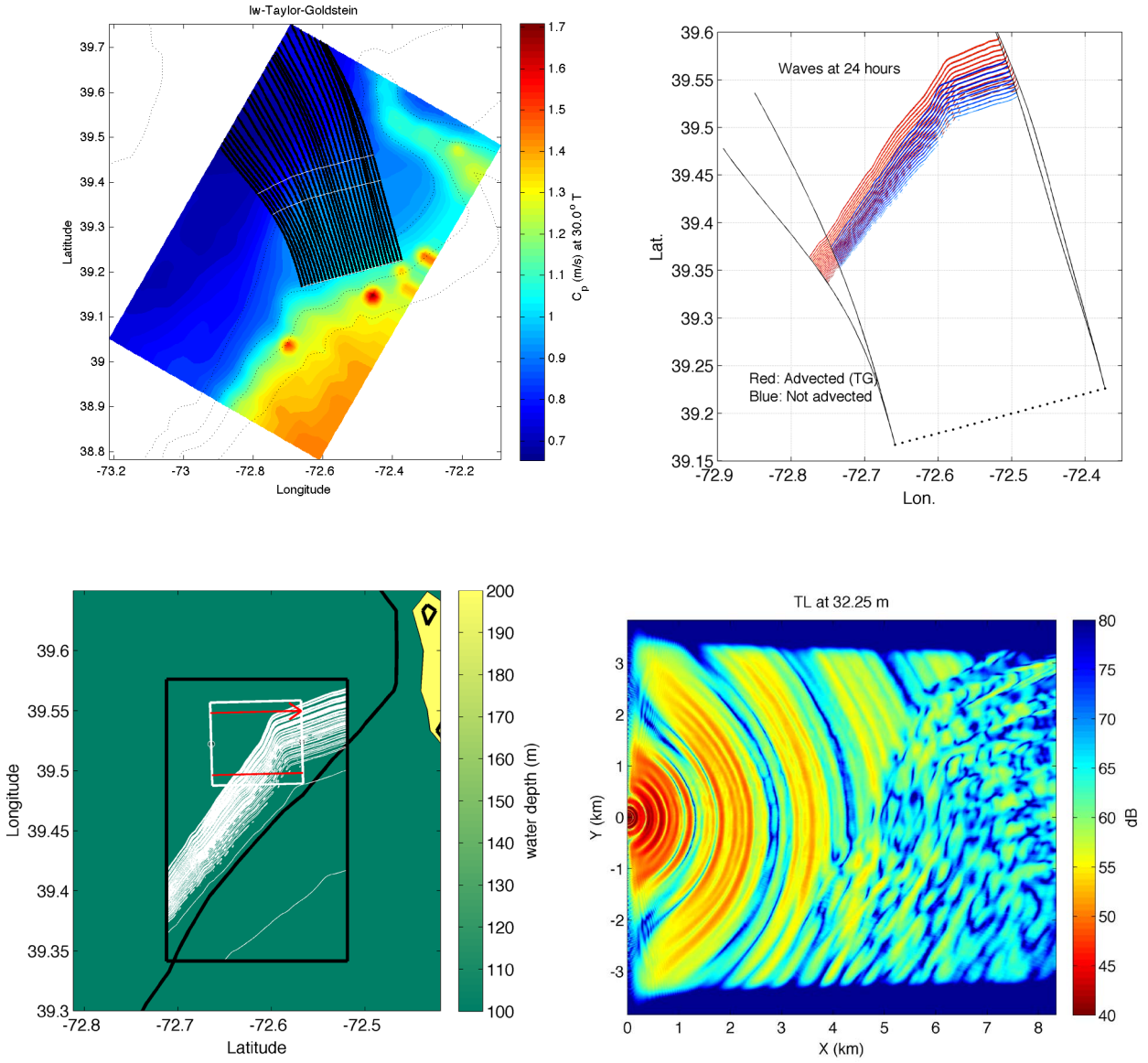

Figure 10. (upper left). Internal-tide rays computed from a detided three-day portion of the 2006 MSEAS reanalysis simulation (Figure 4 shows internal tides that were removed), with advection of the rays included (calculated using Taylor-Goldstein long wave mode-one speeds). Hudson Canyon is seen at the right. (upper right) A snapshot of short-wavelength internal waves computed along the rays with the eKdVf model and a sine-wave starter is shown (synthetic SAR pictures, surface convergences, are shown). Waves computed with advection omitted and with the Taylor-Goldstein long wave advection method are shown. (lower left) A domain for a 200-Hz 3D parabolic equation computation through the with-advection wavefield is shown with a white box, with the waves also shown in white. (lower right) Transmission loss at 32.25 m depth is plotted. The pattern shows cylindrical symmetry away from the strong internal waves, and a more complex structure in the strong internal waves.

IMPACT/APPLICATIONS

The creation of a modeling suite that includes submesoscale features as well as data assimilation is expected to be a valuable asset to apply in numerous ocean regions. Identification of acoustic propagation and noise field features that are controlled by local oceanographic processes may allow exploitation or mitigation of the effects.

An MIT analytical acoustic model, described last year, enables prediction of the temporal coherence time scale and Doppler-shift of acoustic field fluctuations after propagating through a fluctuating ocean waveguide with random 3D surface and internal gravity waves.

TRANSITIONS

The MSEAS random noise ocean process models from MIT are being transitioned to NRL. The process of inserting the virtual seafloor internal-tide parameterization into global ocean and global climate models is being investigated by the NOAA Geophysical Fluid Dynamics Laboratory.

RELATED PROJECTS

There are many closely related projects among the many co-PI's. Some of the acoustics PI's have ONR grants related to shallow-water acoustics. Several of the ocean dynamical modeling PI's have closely related projects on data assimilation, dynamical processes, and/or model development funded by both ONR and the National Science Foundation.

REFERENCES

[1] Thomson, D. J. and N. R. Chapman, N. R., A wide-angle split-step algorithm for the parabolic equation, J. Acoust. Soc. Am., 74, 1848-1854, 1983.

[2] Feit, M. D., and J. A. Fleck, Jr., Light propagation in graded-index fibers, Appl. Opt., 17, 3990-3998, 1978.

[3] Khatiwala, S., Generation of internal tides in an ocean of finite depth: analytical and numerical calculations, Deep-Sea Research I, *50*(1), 3–21, doi:10.1016/S0967-0637(02)00132-2, 2003.

[4] Legg, S., and K. M. H. Huijts, Preliminary simulations of internal waves and mixing generated by finite amplitude tidal flow over isolated topography. *Deep-Sea Research II*, *53*(1-2), 140–156. doi:10.1016/j.dsr2.2005.09.014, 2006.

[5] Klymak, J. M., and J. N. Moum. Internal solitary waves of elevation advancing on a shoaling shelf, Geophys. Res. Lett., 30(20), 2003.

[6] Shchepetkin, A. F. and J. C. McWilliams, Computational kernel algorithms for fine-scale, multiprocess, long-term oceanic simulations. *Handbook of Numerical Analysis. XIV: Computational Methods for the Ocean and the Atmosphere*, P. G. Ciarlet, T. Temam, and J. Tribbia, Eds., Elsevier Science, 119-182, 2008.

[7] Gerkema, T., C. Staquet, and P. Bouruet-Aubertot, Decay of semi-diurnal internal-tide beams due to subharmonic resonance. Geophys. Res. Lett., 33, L08604, 2006.

[8] King, B., H. P. Zhang, and H. L. Swinney, Tidal flow over three-dimensional topography generates out-of-forcing-plane harmonics, Geophys. Res. Lett., 37, L14606, 2010.

[9] Tang, D. J., J. N. Moum, J. F. Lynch, P. Abbot, R. Chapman, P. Dahl, T. Duda, G. Gawarkiewicz, S. Glenn, J. A. Goff, H. Graber, J. Kemp, A. Maffei, J. Nash and A. Newhall, Shallow Water 2006: a joint acoustic propagation/nonlinear internal wave physics experiment, Oceanography, 20(4), 156-167, 2007.

[10] Holloway, P. E., E. Pelinovsky, and T. Talipova, A generalized Korteweg-de Vries model of internal tide transformation in the coastal zone, J. Geophys. Res., 104, 18,333-18,350, 1999.

[11] Jackson, C. R., "*An Atlas of Internal Solitary-Like Waves and Their Properties, 2nd ed*.," Global Ocean Associates, Alexandria, VA, 2004. http://www.internalwaveatlas.com/Atlas2_index.html .

PUBLICATIONS

Badiey, M., L. Wan and A. Song, Three-dimensional mapping of internal waves during the Shallow Water 2006 experiment, J. Acoust. Soc. Am., 134, EL7-EL13, dx.doi.org/10.1121/1.4804945, 2013. [published, refereed]

Colin, M. E. G. D., T. F. Duda, L. A. te Raa, T. van Zon, P. J. Haley Jr., P. F. J. Lermusiaux, W. G. Leslie, C. Mirabito, F. P. A. Lam, A. E. Newhall, Y.-T. Lin , and J. F. Lynch, Time-evolving acoustic propagation modeling in a complex ocean environment, in Proceedings of Oceans '13 (Bergen) Conference, IEEE/MTS, 2013. [published, not refereed]

Dettner, A., H. L. Swinney, and M. S. Paoletti, Internal wave and boundary current generation by tidal flow over topography, Physics of Fluids, 25, 1-15, doi.org/10.1063/1.4826984, 2013. [published refereed]

Duda, T. F., Theory and observation of anisotropic and episodic internal wave effects on 100-400 Hz sound, in Proceedings of the International Conference and Exhibition on Underwater Acoustic Measurements: Technologies and Results, Kos, Greece, pp. 999-1006, 2011. [published, not refereed]

Duda, T. F., Plenary presentation: Identifying and meeting new challenges in shallow-water acoustics, in Proceedings of Acoustics 2013 (AAS2013), Science, Technology and Amenity, Australian Acoustical Society, 2013. [published, not refereed]

Duda, T. F., Y.-T. Lin and D. B. Reeder, Observationally constrained modeling of sound in curved ocean internal waves: Examination of deep ducting and surface ducting at short range, J. Acoust. Soc. Am., 130, 1173-1187, dx.doi.org/10.1121/1.3605565, 2011. [published, refereed]

Duda, T., Y.-T. Lin and B. D. Cornuelle, Scales of time and space variability of sound fields reflected obliquely from underwater slopes, Proc. Meet. Acoust., 19, 070025, 2013. [published, not refereed]

Duda, T. F., Y.-T. Lin, A, E, Newhall, K. R. Helfrich, W. G. Zhang, M. Badiey, P. F. J. Lermusiaux, J. A, Colosi and J. F. Lynch, The "Integrated Ocean Dynamics and Acoustics" (IODA) hybrid modeling effort, in Proceedings of the 2nd International Underwater Acoustics Conference, Rhodes, Greece, 2014. [published, not refereed]

Duda, T. F., W. G. Zhang, and Y.-T.-Lin, Studies of internal tide generation at a slope with nonlinear and linearized simulations: Dynamics and implications for ocean acoustics, in Proceedings of Oceans '12 (Hampton Roads) conference, MTS/IEEE, 2012. [published, not refereed]

Duda, T. F., W. G. Zhang, K. R. Helfrich, A. E. Newhall, Y.-T. Lin, and J. F. Lynch, Issues and progress in the prediction of ocean submesoscale features and internal waves, in Proceedings of Oceans '14 (St. John's) conference, IEEE/MTS, 2014. (9 pp.) [published, not refereed]

Emerson, C., J. F. Lynch, P. Abbot, Y.-T. Lin, T, F. Duda, G. G. Gawarkiewicz, and C.-F. Chen, Acoustic propagation uncertainty and probabilistic prediction of sonar system performance in the southern East China Sea continental shelf and shelfbreak environments, IEEE J. Oceanic Eng., in press, 2014. [in press, refereed]

Gong, Z., T. Chen, P. Ratilal, and N. C. Makris, Temporal coherence of the acoustic field forward propagated through a continental shelf with random internal waves, J. Acoust. Soc. Am., 134, 3476-3485, 2013. [published, refereed]

Grimshaw, R., C. Guo, K. Helfrich, and V. Vlasenko, Combined effect of rotation and topography on shoaling oceanic internal solitary waves, J. Phys. Oceanogr., 44, 1116-1132, 2014. [published, refereed]

Haley, P. J. Jr., A. Agarwal, and P. F. J. Lermusiaux, Optimizing velocities and transports for complex coastal regions and archipelago. Ocean Modeling, in review, 2014. [submitted]

Kiara, A., K. Hendrickson and D. K. P. Yue, SPH for incompressible free-surface flows. Part II: Performance of a modified SPH method, Computers and Fluids, 86, 510-536, dx.doi.org/10.1016/j.compfluid.2013.07.016, 2013. [published, refereed]

King, B., M. Stone, H. P. Zhang, T. Gerkema, M. Marder, R. B. Scott, and H. L. Swinney, Buoyancy frequency profiles and internal semidiurnal tide turning depths in the oceans, J. Geophys. Res. (Oceans) 117, C04008, dx.doi.org/10.1029/2011JC007681, 2012. [published, refereed]

Lee, F. M., M. S. Paoletti, H. L. Swinney, and P. J. Morrison. Experimental determination of radiated wave power without pressure field data, Physics of Fluids, 26, 046606, doi: 10.1063/1.4871808, 2014. [published, refereed]

Lin, Y.-T. and T. F. Duda, A higher-order split-step Fourier parabolic-equation sound propagation solution scheme, J. Acoust. Soc. Am., 132, EL61-EL67, 2012. [published, refereed]

Lin, Y.-T., J. M. Collis, and T. F. Duda, A three-dimensional parabolic equation model of sound propagation using higher-order operator splitting and Padé approximants, J. Acoust. Soc. Am., 132, EL364-370, dx.doi.org/10.1121/1.4754421, 2012. [published, refereed]

Lin, Y.-T., T. F. Duda, and A. E. Newhall, Three-dimensional sound propagation models using the parabolic-equation approximation and the split-step Fourier method, J. Comput. Acoust., 21, 1250018, dx.doi.org/10.1142/S0218396X1250018X, 2013. [published, refereed]

Lin, Y.-T., T. F. Duda, C. Emerson, G. Gawarkiewicz, A. E. Newhall, B. Calder, J. F. Lynch, P. Abbot, Y.-J. Yang and S. Jan, Experimental and numerical studies of sound propagation over a submarine canyon northeast of Taiwan, IEEE J. Oceanic Eng., in press, 2014, http://dx.doi.org/10.1109/JOE.2013.2294291. [in press, refereed]

Lin, Y.-T, K. G. McMahon, J. F. Lynch, and W. L. Siegmann, Horizontal ducting of sound by curved nonlinear internal gravity waves in the continental shelf areas, J. Acoust. Soc. Am., 133, 37-49, dx.doi.org/10.1121/1.4770240, 2013. [published, refereed]

Lynch, J. F., T. F. Duda and J. A. Colosi, Acoustical horizontal array coherence lengths and the "Carey Number", Acoustics Today, 10, 10-19, http://dx.doi.org/10.1121/1.4870172, 2014. [published, not refereed]

Lynch, J. F., T. F. Duda, W. L. Siegmann, J. Holmes and A. E. Newhall, The Carey Number in shallow water acoustics, in Proceedings of the 1st International Underwater Acoustics Conference, Corfu, Greece, 2013. [published, not refereed]

Lynch, J. F., Y.-T. Lin, T. F. Duda and A. E. Newhall , Characteristics of acoustic propagation and scattering in marine canyons, in Proceedings of the 1st International Underwater Acoustics Conference, Corfu, Greece, 2013. [published, not refereed]

Nash, J., S. Kelly, E. Shroyer, J. Moum and T. Duda, The unpredictability of internal tides in coastal seas, In Proc. 7th International Symposium on Stratified Flows, Rome, Italy, 2011. [published, not refereed]

Nash, J. D., S. M. Kelly, E. L. Shroyer, J. N. Moum, and T. F. Duda, The unpredictable nature of internal tides and nonlinear waves on the continental shelf, J. Phys. Oceangr., 42, 1981-2000, dx.doi.org/10.1175/JPO-D-12-028.1, 2012. [published, refereed]

Nash, J. D., E. L. Shroyer, S. M. Kelly, M. E. Inall, T. F. Duda, M. D. Levine, N. L. Jones, and R. C. Musgrave, Are any coastal internal tides predictable? Oceanography, 25, 80-95, http://dx.doi.org/10.5670/oceanog.2012.44, 2012. [published, refereed]

Pan, Y. and D. Yue, Direct numerical investigation of turbulence of capillary waves, Phys. Rev. Lett., 113, 094501, 2014. [published, refereed]

Paoletti, M. S., and H. L. Swinney, Propagating and evanescent internal waves in a deep ocean model, J. Fluid Mech., 108, 148101, dx.doi.org/10.1017/jfm.2012.284, 2012. [published, refereed]

Paoletti, M. S., M. Drake, and H. L. Swinney, Internal tide generation in nonuniformly stratified deep oceans, J. Geophys. Res. Oceans, 119, 1953-1956, doi:10.1002/2013JC009469, 2014. [published, refereed]

Phadnis, A., Uncertainty Quantification and Prediction for Non-autonomous Linear and Nonlinear Systems. SM Thesis, Massachusetts Institute of Technology, Department of Mechanical Engineering, July 2013. [published, not refereed]

Raghukumar, K., and J. A. Colosi, High frequency normal mode statistics in a shallow water waveguide: The effect of random linear internal waves, J. Acoust. Soc. Am. 136 , 66-79, http://dx.doi.org/10.1121/1.4881926, 2014. [published, refereed]

Tran, D. D., M. Andrews, and P. Ratilal, Probability distribution for energy of saturated broadband ocean acoustic transmission: Results from Gulf of Maine 2006 Experiment, J. Acoust. Soc. Am., 132, 3659-3672, 2012. [published, refereed]

Xiao, W., Y. Liu, G. Wu and D. K. P. Yue, Rogue wave occurrence and dynamics by direct simulations of nonlinear wave-field evolution, J. Fluid Mech., 720, 357-392, 2013. [published, refereed]

Zhang, L. and H. L. Swinney, Virtual seafloor reduces internal wave generation by tidal flow, Phys. Rev. Lett., 112, 104502 (2014) doi: 10.1103/PhysRevLett.112.104502, 2014. [published, refereed)

Zhang, W. G. and T. F. Duda, Intrinsic nonlinearity and spectral structure of internal tides at an idealized Mid-Atlantic Bight shelfbreak, J. Phys. Oceanogr., 43, 2641-2660, 2013. [published, refereed]

Zhang, W. G., T. F. Duda, and I. A. Udovydchenkov, Modeling and analysis of internal-tide generation and beam-like onshore propagation in the vicinity of shelfbreak canyons, J. Phys. Oceanogr., 44, 834-849, 2014. [published, referred]